Heliyon 10 (2024) e23197

Contents lists available at ScienceDirect

Heliyon

journal homepage: www.cell.com/heliyon

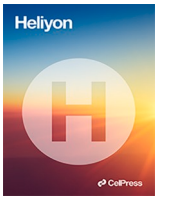

Design and simulation of nitrogenated holey graphene (C_2N) based heterostructure solar cell by SCAPS-1D

Tasnimul Islam Taseen, M. Julkarnain *, Abu Zafor Md Touhidul Islam

Department of Electrical and Electronic Engineering, University of Rajshahi, Rajshahi, 6205, Bangladesh

ARTICLE INFO

Keywords:
C_2N
BSF layer
Solar cells
CZT
SCAPS-1D
Photovoltaics
PCE

ABSTRACT

The nitrogenated holey Graphene (C_2N) based solar cell has been modeled and analyzed by using SCAPS-1D. Initially, a reported structure (TCO/IGZO/C_2N) has been considered and improved by incorporating Al and Pt as front and back contact, respectively. Then, a novel device structure (Al/TCO/IGZO/C_2N/CZT/Pt) has been proposed by inserting a BSF layer with heavily doped p-CZT material. The outcomes of the suggested cell structure have been analyzed numerically by changing different physical parameters. The absorber and BSF layer's thickness has been optimized as 0.6 μm and 0.4 μm, respectively. The cell performance is significantly declined when the bulk defect density in C_2N exceeds the value of 10^{15} cm^{-3}. The rising of device operating temperature shows a negative effect on performance. From this analysis, the structure has been optimized according to device performance. The optimized results have been achieved with the V_{OC}, J_{SC}, FF and efficiency (eta) of 1.40 V, 22.59 mA/cm^2, 89.02%, and 28.16%, respectively. This research contributes to enriching the knowledge on the field of C_2N materials and its use in optoelectronic applications.

1. Introduction

The global energy demand is growing daily as civilization advances. The search for alternative, environmentally friendly, sustainable energy sources has been more widespread in recent years as a result of the growing energy demand, the ongoing burning of fossil energy supplies, and their effects on the environment. Solar energy is becoming more and more well-liked as a plentiful and long-lasting source of renewable energy sources [1,2]. Solar energy is a valuable renewable resource that need to be utilized efficiently for the betterment of the environment. The abundance of solar radiation and its characteristics indicates that the renewable energy is an emerging field of study. Many materials have been researched and produced for solar cells, including Si, CdTe, perovskite, and others that have successful commercial products and high photovoltaic efficiencies [3–12]. However, these materials are toxic and have a few limitations that inhibit them from developing further. The perovskite solar cells are unstable due to their volatile organic components. The usage of Indium, Gallium, or Tellurium, which are scarce materials, drives up the cost of manufacturing CIGS and CdTe. The novel holey nitrogenized material C_2N has effectively been fabricated by a straightforward chemical reaction [13], which opens the doors for using these materials for optoelectronic applications. Usually, layered C_2N has uniform holes and nitrogen atoms [14–16]. It has excellent structural stability and a wider energy bandgap that ranges from 1.7 eV to 1.96 eV [13]. Several theoretical simulations have been conducted on C_2N materials and proposed that C_2N might possess exceptional electrical and optical properties [17–19]. The

* Corresponding author.
E-mail address: jnain.apee@ru.ac.bd (M. Julkarnain).

https://doi.org/10.1016/j.heliyon.2023.e23197
Received 21 July 2023; Received in revised form 24 November 2023; Accepted 29 November 2023
Available online 3 December 2023

distinctive structure and high surface-to-volume ratio of this material make it promising for numerous fields, including hydrogen storage, batteries, sensors, and catalysts [20–26]. In addition, C_2N is a viable option for photovoltaics because of its favorable bandgap, higher absorption coefficient, environmentally nonthreatening, and excellent thermal stability [18,27]. However, there is no extensive studies in this area up to this point. Moreover, the C_2N ayer has not been embedded in solar cell fabrication, and the majority of papers are restricted to reporting their fundamental properties [16–19]. Therefore, it is essential to research the C_2N-based solar cell's characteristics to guide future development. Solar cells simulation is an initial step toward fabricating new cells. In this regard, researchers are focused on the simulation of C_2N-based solar cells and obtained a noticeable result [16,28]. X. Zhou et al. [28] designed and simulated a C_2N-based solar cell with SCAPS-1D software and optimized the window layer. He achieved the best performance (over 17 %) for C_2N/CdS heterojunction solar cells. S. Yasin et al. [16] considered different types of buffer layers (MZO, PCBM, IGZO, $Cd_{0.5}Zn_{0.5}S$) for C_2N-based solar cells. He optimized the buffer layer of a C_2N-based solar cell by SCAPS-1D and obtained the best efficiency of 18.57 % for the IGZO buffer layer.

In this study, a solar cell with C_2N-absorber which was reported by Yasin et al. [16] has been reproduced and modified by adding contact layers and inserting a BSF layer. The reported structure (TCO/IGZO/C_2N/back contact) has been firstly improved by incorporating Al and Pt as the front and back contact, respectively. Then, a comparatively highly doped CZT is inserted as a BSF layer between the C_2N and Pt to enhance the performance of the cell. The proposed hetero-junction structure becomes Al/TCO/IGZO/C_2N/CZT/Pt. The cell structure Al/TCO/IGZO/C_2N/Pt and Al/TCO/IGZO/C_2N/CZT/Pt is referred to as the cell (i) without BSF layer and (ii) with BSF layer, respectively. The device structures have been analyzed by changing physical parameters of different layers and operating temperature.

2. Modeling and physical parameters

The SCAPS-1D, created by a team at the Department of Electronics and Information Systems (ELIS), University of Gent, Belgium [29,30], has been used to numerically simulate this study. The continuity equations for free electrons and holes as well as Poisson's equation are the three key equations of semiconductor physics considered to develop this software. The key equations; Poisson equation (Equation (1)), continuity equation for electrons (Equation (2)), and continuity equation for holes (Equation (3)) are used for semiconductor device simulation and shown below [29,30]:

Poisson equation:

$$\frac{\partial}{\partial x}\left(\varepsilon_0\varepsilon_r\frac{\partial \psi}{dx}\right) = -q\left(p - n + N_D^+ - N_a^- + \frac{\rho}{q}\right) \tag{1}$$

Continuity equation for electrons:

$$-\left(\frac{1}{q}\right)\frac{\partial J_n}{\partial x} - U_n + G = \frac{\partial n}{\partial t} \tag{2}$$

Continuity equation for holes:

$$-\left(\frac{1}{q}\right)\frac{\partial J_p}{\partial x} - U_p + G = \frac{\partial p}{\partial t} \tag{3}$$

where Ψ represents the wave function for the electrostatic potential, n and p are the electrons and holes concentrations, respectively, G

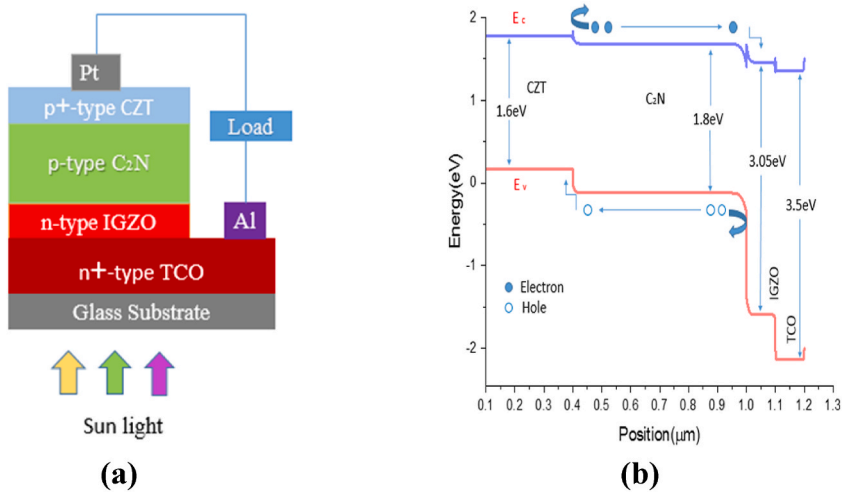

Fig. 1. The schematic (a) block diagram (b) corresponding band diagram of the C_2N-based solar cell.

Table 1
Physical parameters of proposed C_2N solar cell [13,16,28,32].

Parameters (Unit)	n-TCO (Window)	n-IGZO (Buffer)	p-C_2N (Absorber)	p-CZT (BSF)
Thickness, W (μm)	0.1	0.1	0.5*	0.1*
Energy bandgap, E_g (eV)	3.5	3.05	1.8	1.6
Affinity of electron, χ(eV)	4	4.16	4.42	4.5
Dielectric permittivity, ε_r	10	10	4.5	11
Density of states N_C (cm^{-3})	2.2×10^{18}	5×10^{18}	10^{19}	10^{16}
Density of states, N_V (cm^{-3})	1.8×10^{18}	5×10^{18}	10^{19}	10^{17}
Thermal velocity of electron (cm/s)	10^7	10^7	10^7	10^7
Thermal velocity of hole (cm/s)	10^7	10^7	10^7	10^7
Mobility of electron, μ_e (cm^2/Vs)	20	15	13	960
Mobility of hole, μ_p (cm^2/Vs)	10	0.1	20.6	56
Donor Concentration, n (cm^{-3})	2×10^{19}	10^{18}	0	0
Acceptor Concentration, p (cm^{-3})	0	0	10^{17}	7.5×10^{19}
Type of Defect	Neutral	Neutral	Neutral	Neutral
Density of Defect, N_t(cm^{-3})	10^{14}	10^{15}	10^{15}	10^{14}
Energy Distribution	single	Single	Gaussian	Single
Absorption coefficient	SCAPS	SCAPS	SCAPS	SCAPS

Note: * denotes variable fields.

is the generation rate, and N_D+ and N_A-are the ionized donors and acceptors densities, $\mathcal{E}_0$ and $\mathcal{E}_r$ are the permittivity of free space and the relative permittivity, and ρ is the density of defects. The current densities for electrons and holes are J_n and J_p, respectively.

The SCAPS-1D can operate in a variety of situations: including back contact voltage, illumination in both light and dark, cell operating temperature, putting diverse interface conditions. All of these simulations were run with the light of the worldwide AM 1.5 spectrum and at a temperature of 300 K. We concentrate on the computed outcomes for this study.

The general design of the C_2N-based solar cell has been modeled by considering the earlier reported structure [16] and modified by including Al and Pt as front and back contact, respectively. The modified structure (Al/TCO/IGZO/C_2N/Pt) is referred to as a cell (i) without a BSF layer. To improve the performance of the cell, a highly doped CZT is inserted as a BSF layer between the C_2N and Pt. This proposed structure (Al/TCO/IGZO/C_2N/CZT/Pt) is referred to as cell (ii) with a BSF layer. The device's absorber layer is made of nitrogenated holey C_2N-based material, and its layer structure is as follows: Glass substrate with metal front contact (Al), TCO, buffer layer, absorber layer, and back surface field (BSF) layer and back contact (Pt) layer. We considering Indium Gallium Zinc Oxide (IGZO) as the buffer layer and Cadmium Zinc Telluride (CZT) as the BSF layer. The charge gradient on the same type of semiconductor produces a built-in potential. Based on this concept, a p + semiconductor is positioned amid the absorber and the back contact. The p + -semiconductor layer is referred to as the BSF layer, and the field is referred to as the back surface field (BSF) [31]. The proposed cell and its energy band structure extracted from SCAPS-1D are shown in Fig. 1(a) and (b), respectively. The fundamental physical parameters for this simulation are considered from earlier reports and listed in Tables 1 and 2 [13,16,28,32]. The value of the absorption coefficient α(λ) of each layer needs to be inserted in SCAPS-1D software. This can be included by either absorption file (.abs) or calculated by using different built-in models stated in the optical absorption α(λ) of materials in the SCAPS manual [30]. Here we choose the SCAPS model "Eg-sqrt" (Equation (4)) for the optical absorption $\alpha(h\nu)$ calculation of different layers:

$$\alpha(h\nu) = \left(\alpha_0 + \beta_0 \frac{E_g}{h\nu}\right)\sqrt{\frac{h\nu}{E_g} - 1} \tag{4}$$

here, E_g is the bandgap of the material in eV, $h\nu$ is the energy of a photon in eV, and the model constants α_0 and β_0 (1/cm). The bandgap (E_g) value of C_2N material is chosen as 1.80 eV extracted from Refs. [16,28] and the model constants α_0 and β_0 are considered as $1.342 \times 10^5 cm^{-1}$ and $1.0 \times 10^{-12} cm^{-1}$, respectively. By examining the impact of thickness, defect density, and doping density on the device performance, the different layers have been optimized.

From SCAPS-1D output, the diagram of the energy band can be derived, and Fig. 1(b) shows the corresponding diagram of the suggested cell with CZT BSF. Two forms of conduction band offset are created at the absorber/emitter contact depending on the material's quality and properties: (i) a "spike type" (positive offset, +ΔEc) and (ii) a "Cliff type" (negative offset, -ΔEc). At the C_2N/

Table 2
Defect parameters on IGZO/C2N and C2N/CZT interface.

Parameters	IGZO/C_2N interface	C_2N/CZT interface
Type of defect	Neutral	Neutral
Defect energy level from E_V (eV)	0.6	0.6
Electron's capture cross-section area (cm^2)	10^{-14}	10^{-14}
Hole's capture cross-section area (cm^2)	10^{-17}	10^{-17}
Energetic distribution	Single	Single
Total defect density, N_t (cm^{-2})	10^{11} *	10^{11} *

Note: * denotes variable fields.

Table 3
Physical parameters for front and back contact.

Parameters	Front Contact	Back Contact
Surface recombination velocity, S_e (cm/s)	10^7	10^5
Surface recombination velocity, S_h (cm/s)	10^5	10^7
Work function (eV)	4.32; Al	5.93; Pt

IGZO interface, a positive conduction band offset (spike type) is seen in this instance. Very little band bending is caused by a very slight spike or nearly straight band offset, which enables a higher holes density on the absorber side. The cross-interface recombination may be enhanced by the higher hole density, increasing the recombination current and decreasing V_{OC} [33]. Determining the optimum cell parameters is the main and most important task of a simulation. To do this, several factors, including layer thickness and carrier concentrations, defect densities, etc., have been varied systematically to obtain the optimum performance of the cell.(see Tables 1 and 2)

The contact parameters are taken from earlier reports [31,34,35] and concise in Table 3.

3. Results and discussion

3.1. Improvement of C_2N solar cell by inserting a CZT BSF layer

The proposed cell structures (i) without BSF layer (Al/TCO/IGZO/C_2N/Pt) and (ii) with BSF layer (Al/TCO/IGZO/C_2N/CZT/Pt) have been studied systematically to obtain optimized performance. A reasonable study of J-V and QE characteristics of both cells has been carried out and presented in Fig. 2. From Fig. 2(a), it is revealed that the CZT BSF layer considerably improved the J_{SC} thus the cell performance compared to those of the same solar cell without the BSF layer. The output performance parameters of both the proposed cell structures without and with BSF layer along with the reference and reproduced cell structures have been presented in Table 4. From the table, it is observed that the output parameters of the replicated cell agreed satisfactorily with the reference cell structure [16]. This study validates our present work and opens a window for improving performance. It also reveals that the cell conversion efficiency is improved from 18.22 to 22.10 % by including contact layers and finally to 28.16 % by incorporating the BSF layer. As the open circuit voltage (V_{OC}) and Fill-factor (FF) remain nearly constant after inserting the BSF layer, the enhancement in efficiency is attributed to improving the J_{SC} from 17.82 to 22.59 mA/cm^2. The performance enhancement of this cell can be explicated by the phenomena like electric field due to charge gradient in p-p$^+$ junction, band bending between C_2N and CZT layers, and enhancement in photoconverted carriers.

The minority carriers are repealed away from the back surface due to the built-in potential and hence reduces the back-surface recombination velocity and increases the J_{SC}.

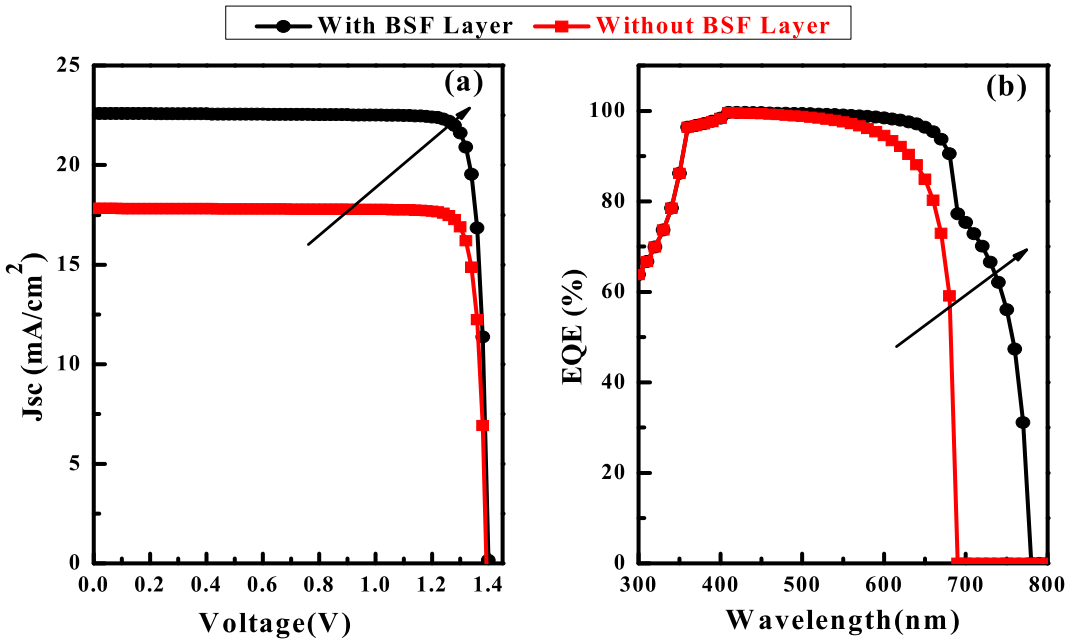

Fig. 2. (a) The simulated current density (J_{SC}) vs. voltage (V) curves and (b) Quantum Efficiency (QE) curves of C_2N-based solar cells with and without BSF layer.

Table 4
A comparison of output parameters of C_2N-based solar cells.

Structures	Performance parameters				Comments
	V_{OC} (V)	J_{SC} (mA/cm^2)	FF (%)	PCE (%)	
Glass/TCO/IGZO/C_2N/back contact	1.22	17.65	84.43	18.22	Reference [16]
Glass/TCO/IGZO/C_2N/back contact	1.20	17.70	85.47	18.15	Reproduced
Al/TCO/IGZO/C_2N/Pt	1.39	17.82	88.95	22.10	Proposed without BSF
Al/TCO/IGZO/C_2N/CZT/Pt	1.40	22.59	89.02	28.16	Proposed with BSF

The formation of preferable band offset among the CZT BSF and C_2N absorber blocks the photo-generated electrons and reflected them to the front contact. Thus, incorporating the BSF layer into the solar cell results in the formation of favorable band alignment between the conduction and valance bands which assists holes whereas hinders electrons to reach the back contact [31,36,37].

In the case of cells with BSF, the BSF layer also act as absorber which enhances the electron-hole pair generation. The quantum efficiency (QE) curve of the proposed cell is shown in Fig. 2(b) elucidates that introducing BSF layer enhances the QE in the longer wavelength (600–800 nm) region which improves the cell performance.

3.2. C_2N absorber layer optimization

3.2.1. Effect of thickness and doping concentration of C_2N absorber layer on PV solar cell

Fig. 3 shows the observed and portrayed effects of thickness and doping concentration of the absorber layer on device output parameters. The doping concentration varies between 10^{12} and 10^{18} cm^{-3}, while the absorber layer's thickness varies from 0.5 to 1.5 μm. The V_{oc}, efficiency, and FF increase with increasing doping concentration, while the J_{sc} decreases along with it. All the parameter values decrease with rising the absorber thickness. The functioning of a cell is significantly persuaded by the thickness of the absorber

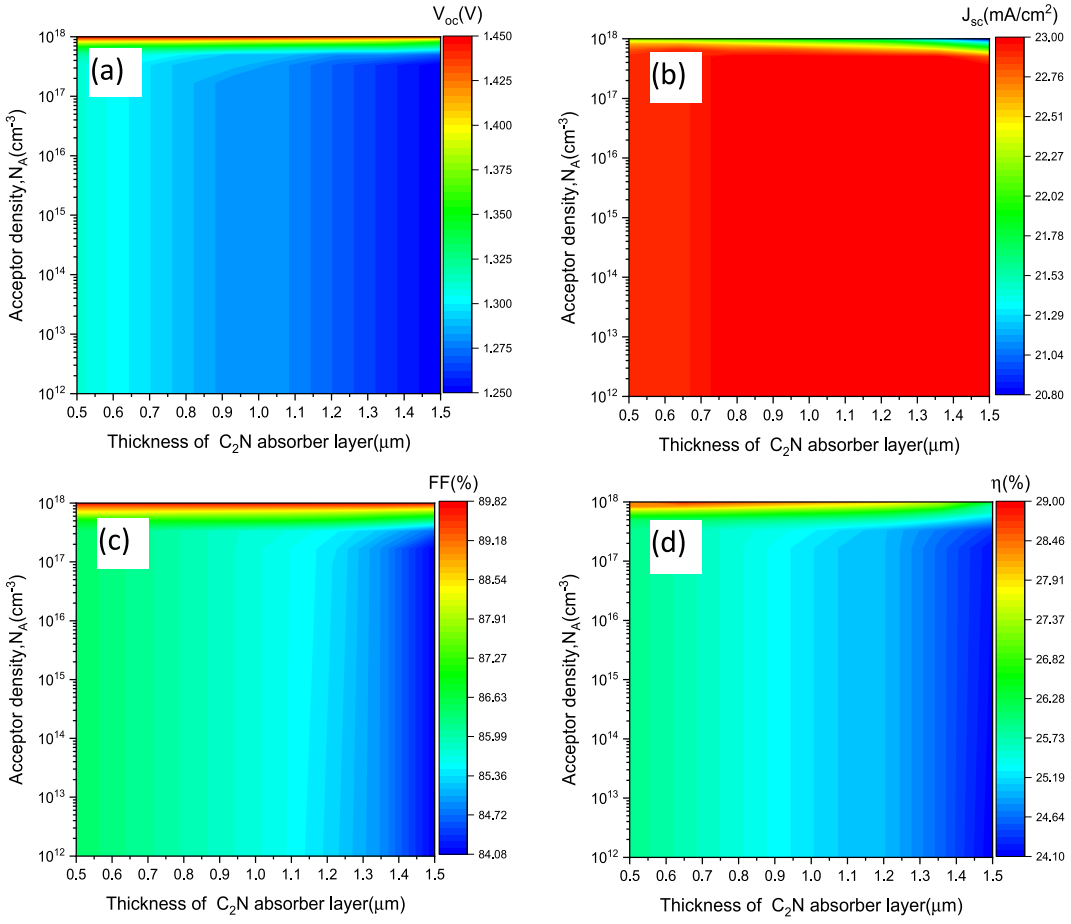

Fig. 3. Variation of photovoltaic output parameters: (a) V_{OC}, (b) J_{SC}, (c) FF, and (d) Efficiency (η) of C_2N-based solar cell with absorber layer thickness and doping concentration.

layer. It directly affects the charge carriers' diffusion length. The Beer-Lambert rule states that when the path length shortens, the absorbed light's intensity grows exponentially [38]. A few hundred nanometers of absorber film may be absorbed sufficient sun's spectrum to saturate solar efficiency. Here, the efficiency, V_{oc}, and FF start declining above 0.6 μm, whereas J_{sc} becomes saturated. The absorber layer thickness therefore optimized to 0.6 μm. All metrics (V_{oc}, FF, and eta) increase along with the rise in doping concentration, however, J_{sc} seems constant. Thus, considering the production costs and fabrication rates, a doping concentration of 10^{17} cm^{-3} is considered to be the optimized concentration. At this optimized condition, the values of V_{oc}, J_{sc}, FF, and eta are found to be 1.40V, 22.59 mA/cm^2, 89.02 %, and 28.16 %, respectively.

3.2.2. *Influence of cell performance on absorber layer defect density*

The optical characteristics of thin film depends on the quality of the films. The functioning of solar cells is always negatively impacted by defects in their layers. Therefore, it is crucial to monitor the impact of the absorber layer's defect density. To study the effect of the defect density of the absorber layer on cell performance, the defect density of the C_2N layer varies from 10^{12} to 10^{17} cm^{-3}, while the thickness of the absorber layer is simultaneously altered from 0.5 to 1.5 μm. Fig. 4 shows that all of the solar cell's characteristics, including V_{oc}, J_{sc}, FF, and eta, have considerably declined with rising defect density. The defect states act as localized energy levels and serve as a recombination center [39]. Thus, with increasing the defect density, the carrier recombination rate enhances which deteriorates the cell performance. Additionally, higher series resistance and a poor fill factor are caused by increasing defect density. As a result, we have selected an optimum defect density of 10^{15} cm^{-3} with absorber thickness of 0.6 μm. The optimized performance parameters, V_{oc}, J_{sc}, FF, and eta are found to be 1.40V, 22.59 mA/cm^2, 89.02 %, and 28.16 %, respectively.

3.2.3. *Effect of the interface defect density on cell performances*

The interface defect has a significant effect on device performance. Therefore, we must observe the effect of the defects at interface (CZT/C_2N and C_2N/IGZO interfaces) on the output parameter. We changed the defect density at the CZT/absorber interface between 10^{10} and 10^{20} cm^{-2} and its outcomes are presented in Fig. 5(a). A detrimental effect is observed with increasing defect density. From the figure, it is revealed that, up to $10^{11}cm^{-2}$, there had been no appreciable change in the efficiency; but as defect density increased, the efficiency began to deteriorate rapidly. Device performance starts to rapidly degrade at interface defect levels of the order of 10^{11}-

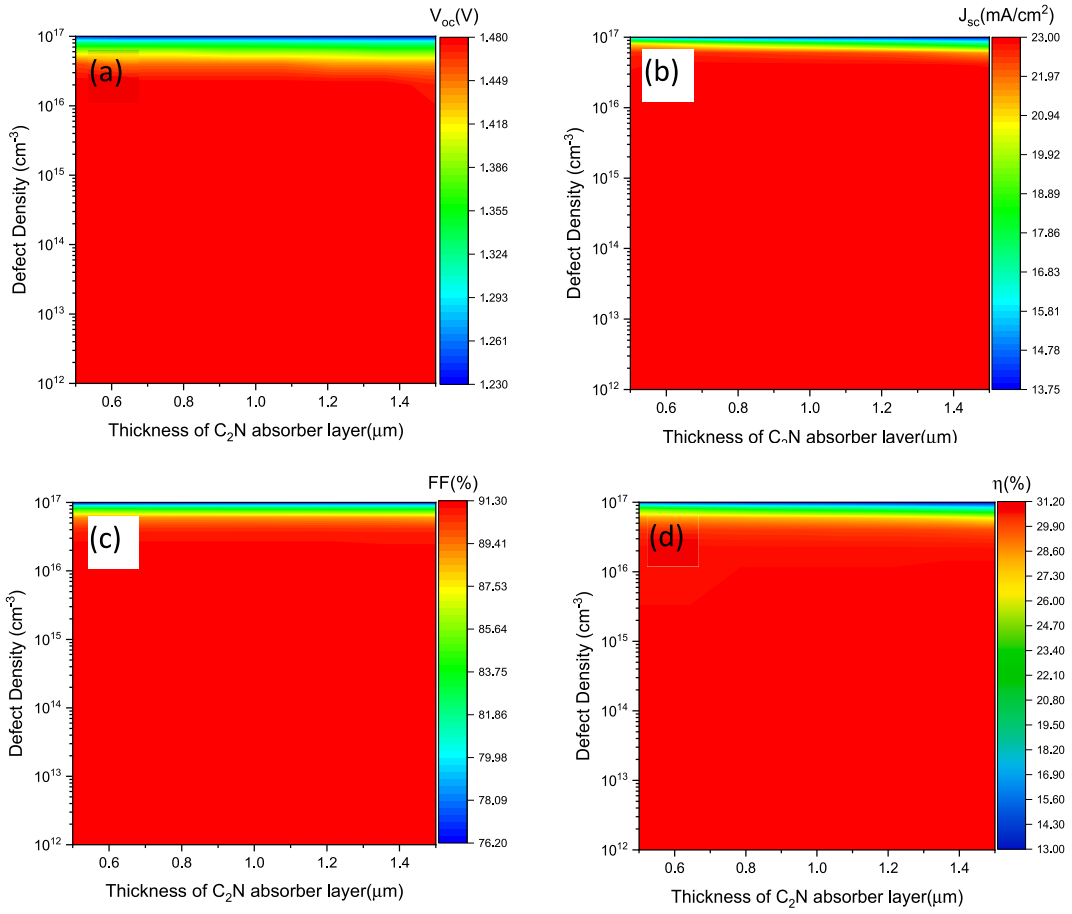

Fig. 4. Variation of photovoltaic performance: (a) V_{OC}, (b) J_{SC}, (c) FF, and (d) Efficiency (η) of SC with thickness and defects density of C_2N layer.

10^{14} cm-^{2} in device layers. The eta value has been reduced from 28.31 % to 18.72 % between 10^{11} and 10^{14} cm^{-2} of the CZT/C_2N interface defect density. The values of all parameters dropped with rising defect density. However, all of the PV characteristics are constant beyond 10^{16} cm^{-2}. Therefore, the CZT/C_2N interface defect density has been considered to be 10^{11} cm^{-2} to achieve optimum solar cell values. Additionally, we changed the density of the interface defects at the C_2N/IGZO interface from 10^{10} to 10^{20} cm^{-2} as shown in Fig. 5(b). A constant efficiency was observed up to 10^{15} cm^{-2} and dropped to 25.32 % from 28.25 % for subsequent increases in defect density to 10^{19} cm^{-2}, and there was a sizable fall in V_{OC} and J_{sc} as well. The Shockley-Read-Hall (SRH) recombination process may help to explain this phenomenon [40]. With increasing defect density carrier lifetime decreases thus carrier recombination is enhanced which deteriorates the efficiency. More carriers are also trapped in the defect sites with increasing defect density. To achieve our intended outcome, we have chosen an optimal density of 10^{11} cm^{-2} for both interfaces.

3.3. Impact of BSF layer thickness and doping concentration on PV solar cell

The solar cell performance has been observed by changing the thickness and doping concentration of the BSF layer. The BSF layer's thickness is changed from 0.1 to 0.6 μm and its impact on cell performance parameters V_{OC}, J_{SC}, FF, and eta is shown in Fig. 6(a). The performance parameters (J_{SC} and eta) increase with increasing the BSF layer thickness. The V_{OC} and FF seem nearly constant in the investigated range, whereas, the J_{SC} rises linearly from 19.7 to 23.1 mA/cm^2 with rising the BSF layer thickness from 0.1 to 0.5 μm. The efficiency also increases from 24.5 to 28.7 % and follows the same pattern of J_{SC}. A similar outcome was reported by other researchers [31,41]. Increasing the efficiency with thickness can be attributed to more electron-hole pairs generation on thick layer. Even though efficiency rises with thickness, 0.4 μm was chosen as the optimum thickness to save the cost of the cells as thick cells are costlier.

Fig. 6 (b) shows the effect of the doping concentration of the BSF layer on various output parameters (V_{OC}, J_{SC}, FF, and eta). All the parameters gradually rise with increasing the doping concentration of the BSF layer from 10^{15} to $10^{19}$$cm^{-3}$, after that all becomes saturated. A gradient in the doping concentration on absorber/BSF layer contact produces the built-in field that repeals the minority carrier from the interface. Thus, the recombination rate at interface is reduced and hence improves efficiency as the doping concentration rises over 10^{17} cm^{-3}. In addition, by lowering the Fermi level and raising the doping concentration, an advantageous band bending developed among the BSF layer and back contact [31,36]. As a consequence, the back contact has a more effective assortment of holes, which improves performance. Due to this research, an optimum doping concentration and thickness were set to be 7.5×10^{19} cm^{-3} and 0.4 μm, respectively.

3.4. Effect of operating temperature on cell performance

The operating device temperature strongly correlates with the stability of solar cell outcomes. According to earlier research, the solar cells performance degrades at higher temperatures. This was mostly ascribed to the layer's quality deformation that instabile the

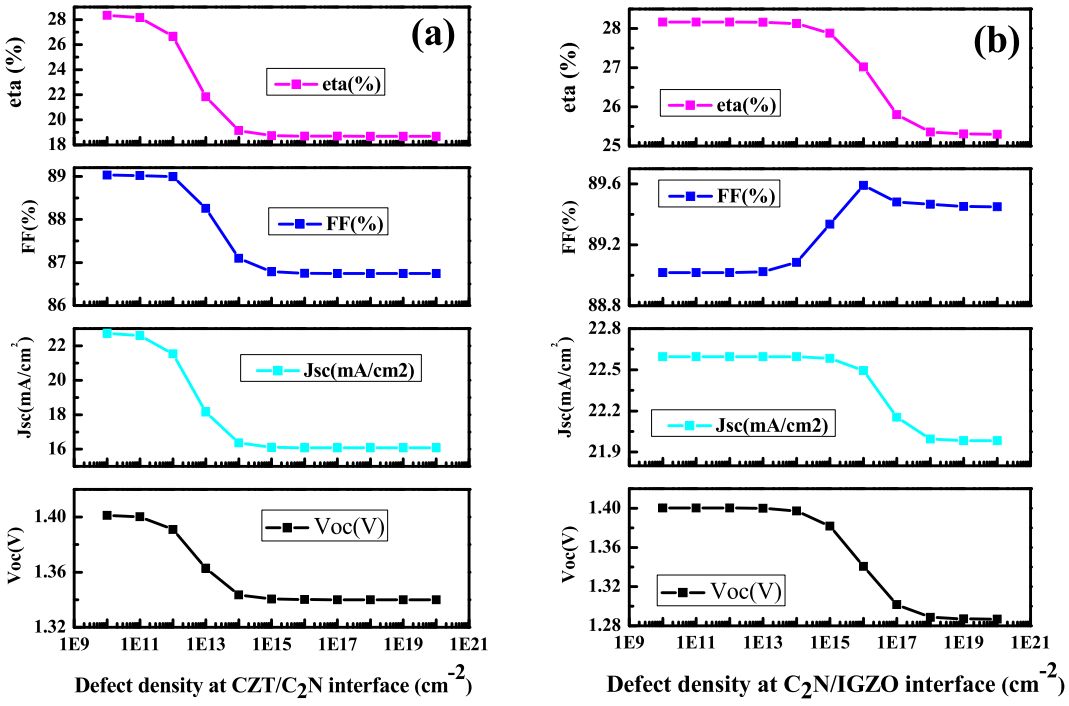

Fig. 5. Variation of PV performance parameters with defect density of (a) CZT/C_2N interface and (b) C_2N/IGMO interface of the of C_2N based solar cell structure.

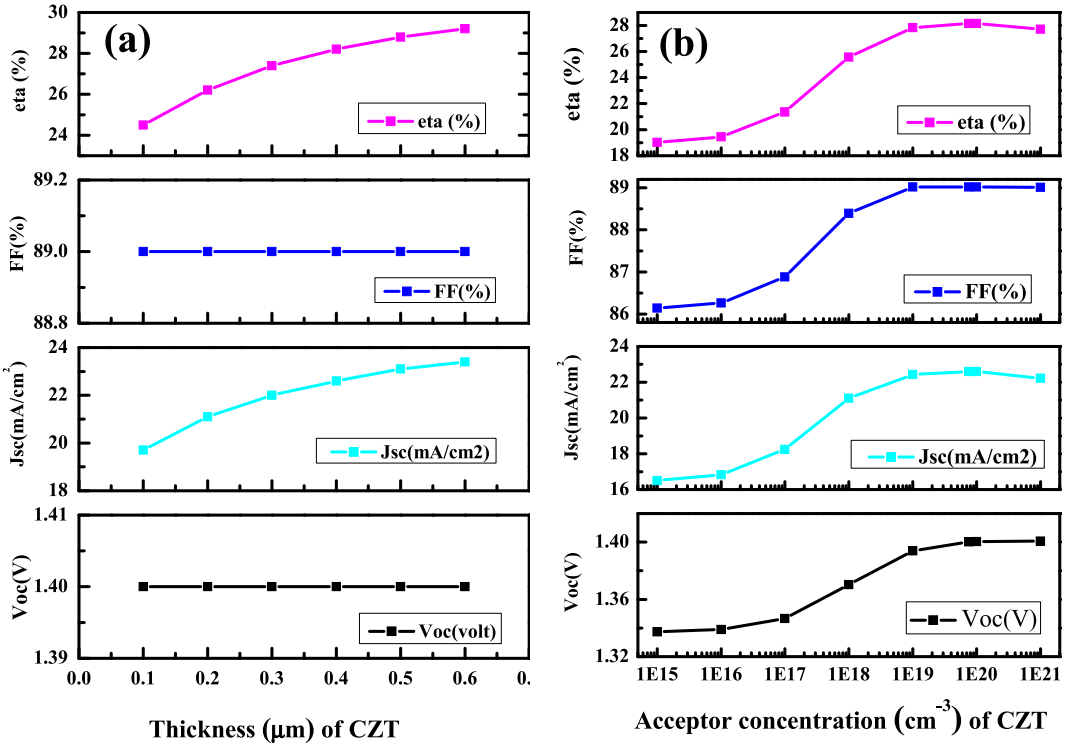

Fig. 6. Variation of photovoltaic output parameters of C_2N-based solar cells with (a) BSF (CZT) layer thickness and (b) BSF (CZT) layer doping concentration.

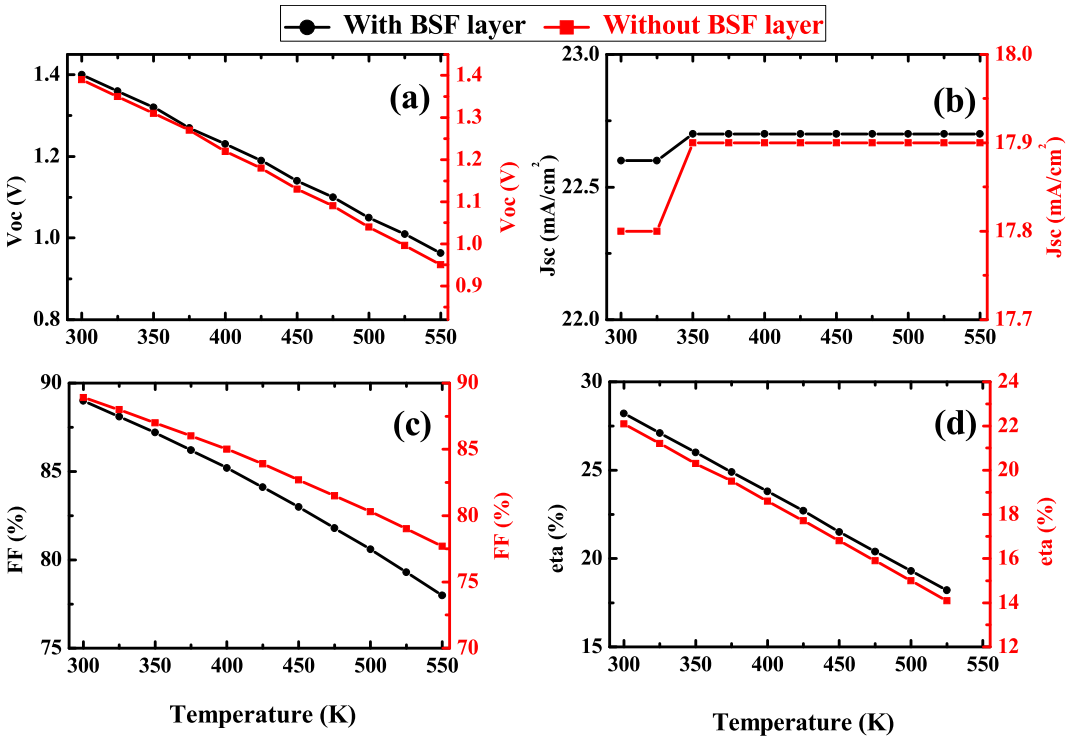

Fig. 7. Output parameters: (a) V_{OC}, (b) J_{SC}, (c) FF, and (d) Efficiency (η) of C_2N based cells with operating temperature.

solar cell structure [42,43]. To observe the effect of device temperature on cell outputs of our suggested structure, the temperature rose from 300 to 550 K for both structures, as depicted in Fig. 7. The V_{oc}, FF, and eta are decreased with increasing the temperature for both the structures. The Jsc indicates a slight improvement in both cases with increasing the temperature. In general, as the operational temperature rises, the energy bandgap of most semiconductors shrinks [44,45], which deteriorates the V_{oc}. Furthermore, the bandgap decreases with increasing temperature, increasing the J_{SC} [36]. Different defect states present in the devices are also activated with increasing temperature which hinders the performance. The decline in V_{OC} and FF is a cause of to drop in efficiency with operational temperature. As a result, we chose 300 K as the ideal temperature because it is simple to maintain in the experimental setting and maintains a comfortable value for all the parameters.

4. Conclusions

The proposed solar cell by using C_2N absorber and CZT BSF layer was examined by SCAPS-1D software. A published cell structure (TCO/IGZO/C_2N/back contact) with an efficiency of 18.22 % has been firstly reproduced and improved by incorporating the Al and Pt as front and back contact materials, respectively. Then, a novel solar cell structure (Al/TCO/IGZO/C_2N/CZT/Pt) is proposed by including a heavily doped p-CZT material as BSF layer. The output parameters of the proposed device structure have been studied numerically by changing different physical parameters like thickness, doping density, and bulk and interfacial defect densities. The cell temperature has also been varied and the performance is noticed to decrease with the increase of temperature. From these numerical analyses, an optimized solar cell device structure has been proposed with 0.6 and 0.4 μm absorber and BSF layer, along with the doping concentrations of 1×10^{17} cm^{-3} and 7.5×10^{19} cm^{-3}, respectively. The efficiency significantly enhanced from 18.22 to 28.16 % by incorporating the BSF layer with enhancement in V_{OC} from 1.3938 to 1.40V, J_{SC} from 17.82 to 22.59 mA/cm^2, and FF from 88.95 to 89.02 %. This research contributes to enriching the knowledge of C_2N materials and their use in solar cells, and suggests that C_2N might be a potential candidate for optoelectronic applications.

Availability of data

Data generated and used for analyses of results presented in this manuscript will be provided by the corresponding author on reasonable requests.

CRediT authorship contribution statement

Tasnimul Islam Taseen: Writing – original draft, Investigation. **M. Julkarnain:** Writing – review & editing, Validation, Formal analysis, Data curation. **Abu Zafor Md Touhidul Islam:** Supervision, Methodology, Conceptualization.

Declaration of competing interest

The authors declare the following financial interests/personal relationships which may be considered as potential competing interests:A Z M Touhidul Islam reports financial support was provided by University of Rajshahi, Bangladesh. M Julkarnain reports a relationship with the University of Rajshahi that includes: employment.

Acknowledgments

The authors acknowledge Dr. Marc Burgelman and his team for providing the SCAPS-1D software.

References

[1] M. Hosenuzzaman, et al., Global prospects, progress, policies, and environmental impact of solar photovoltaic power generation, Renew. Sustain. Energy Rev. 41 (2015) 284–297.
[2] S. Mekhilef, R. Saidur, A. Safari, A review on solar energy use in industries, Renew. Sustain. Energy Rev. 15 (4) (2011) 1777–1790.
[3] X. Wu, High-efficiency polycrystalline CdTe thin-film solar cells, Sol. Energy 77 (6) (2004) 803–814.
[4] M.D. Kelzenberg, et al., Enhanced absorption and carrier collection in Si wire arrays for photovoltaic applications, Nat. Mater. 9 (3) (2010) 239–244.
[5] K. Masuko, et al., Achievement of more than 25% conversion efficiency with crystalline silicon heterojunction solar cell, IEEE J. Photovoltaics 4 (6) (2014) 1433–1435.
[6] J.M. Burst, et al., CdTe solar cells with open-circuit voltage breaking the 1 V barrier, Nat. Energy 1 (3) (2016), 16015.
[7] N.J. Jeon, et al., Compositional engineering of perovskite materials for high-performance solar cells, Nature 517 (7535) (2015) 476–480.
[8] N. Ahn, et al., Highly reproducible perovskite solar cells with average efficiency of 18.3% and best efficiency of 19.7% fabricated via lewis base adduct of lead (II) iodide, J. Am. Chem. Soc. 137 (27) (2015) 8696–8699.
[9] Z. Xiao, et al., Solvent annealing of perovskite-induced crystal growth for photovoltaic-device efficiency enhancement, Adv. Mater. 26 (37) (2014) 6503–6509.
[10] A.A.M. Brown, et al., Lead halide perovskite nanocrystals: room temperature syntheses toward commercial viability, Adv. Energy Mater. 10 (34) (2020), 2001349.
[11] N. Thakur, P. Kumar, P. Sharma, Simulation study of chalcogenide perovskite (BaZrSe3) solar cell by SCAPS-1D, Mater. Today: Proc. (2023).
[12] N. Thakur, et al., Recent advances in BaZrS3 perovskites: synthesis, properties, and future trends, J. Alloys Compd. 957 (2023), 170457.
[13] J. Mahmood, et al., Nitrogenated holey two-dimensional structures, Nat. Commun. 6 (1) (2015) 6486.
[14] Z. Chen, X. Li, J. Yang, The contacts of the monolayer semiconductor C2N with 2D metal electrodes, Advanced Theory and Simulations 2 (3) (2019), 1800161.
[15] H. Zhang, et al., Point defect effects on photoelectronic properties of the potential metal-free C2N photocatalysts: insight from first-principles computations, J. Phys. Chem. C 122 (10) (2018) 5291–5302.
[16] S. Yasin, et al., Optoelectronic simulation of a high efficiency C2N based solar cell via buffer layer optimization, Opt. Mater. 119 (2021), 111364.

[17] J. Xu, et al., 2D frameworks of C2N and C3N as new anode materials for lithium-ion batteries, Adv. Mater. 29 (34) (2017), 1702007.
[18] J. Sun, et al., A many-body GW + BSE investigation of electronic and optical properties of C2N, Appl. Phys. Lett. 109 (13) (2016), 133108.
[19] R.M. Tromer, et al., Atomic adsorption on nitrogenated holey graphene, J. Phys. Chem. C 121 (5) (2017) 3055–3061.
[20] J. Mahmood, et al., An efficient and pH-universal ruthenium-based catalyst for the hydrogen evolution reaction, Nat. Nanotechnol. 12 (5) (2017) 441–446.
[21] C. Li, et al., A promising blue phosphorene/C2N van der Waals type-II heterojunction as a solar photocatalyst: a first-principles study, Phys. Chem. Chem. Phys. 22 (2) (2020) 615–623.
[22] L. Wang, et al., Van der Waals heterostructures comprised of ultrathin polymer nanosheets for efficient Z-scheme overall water splitting, Angew. Chem. Int. Ed. 57 (13) (2018) 3454–3458.
[23] S. Tripathi, et al., Contribution to sustainable and environmental friendly non-toxic CZTS solar cell with an innovative hybrid buffer layer, Sol. Energy 204 (2020) 748–760.
[24] T. Hussain, et al., Sensing of volatile organic compounds on two-dimensional nitrogenated holey graphene, graphdiyne, and their heterostructure, Carbon 163 (2020) 213–223.
[25] Y. Yong, et al., C2N monolayer as NH3 and NO sensors: a DFT study, Appl. Surf. Sci. 487 (2019) 488–495.
[26] A. Hashmi, et al., Ultra-high capacity hydrogen storage in a Li decorated two-dimensional C2N layer, J. Mater. Chem. A 5 (6) (2017) 2821–2828.
[27] A. Bafekry, et al., A first-principles study of the effects of atom impurities, defects, strain, electric field and layer thickness on the electronic and magnetic properties of the C2N nanosheet, Carbon 157 (2020) 371–384.
[28] X. Zhou, J. Han, Design and simulation of C2N based solar cell by SCAPS-1D software, Mater. Res. Express 7 (12) (2020), 126303.
[29] M. Burgelman, P. Nollet, S. Degrave, Modelling polycrystalline semiconductor solar cells, Thin Solid Films 361–362 (2000) 527–532.
[30] K.D. Marc Burgelman, Alex Niemegeers, Johan Verschraegen, Stefaan Degrave, SCAPS Manual, 2023.
[31] M.S. Rana, M.M. Islam, M. Julkarnain, Enhancement in efficiency of CZTS solar cell by using CZTSe BSF layer, Sol. Energy 226 (2021) 272–287.
[32] F. Anwar, et al., Effect of different HTM layers and electrical parameters on ZnO nanorod-based lead-free perovskite solar cell for high-efficiency performance, Int. J. Photoenergy 2017 (2017), 9846310.
[33] T. Song, A. Kanevce, J.R. Sites, Emitter/absorber interface of CdTe solar cells, J. Appl. Phys. 119 (23) (2016), 233104.
[34] M. Dey, et al., Germanium telluride as a BSF material for high efficiency ultra-thin CdTe solar cell, in: 2014 9th International Forum on Strategic Technology (IFOST), 2014.
[35] J. Hölzl, F.K. Schulte, Work function of metals, in: J. Hölzl, F.K. Schulte, H. Wagner (Eds.), Solid Surface Physics, Springer Berlin Heidelberg, Berlin, Heidelberg, 1979, pp. 1–150.
[36] M. Atowar Rahman, Enhancing the photovoltaic performance of Cd-free Cu2ZnSnS4 heterojunction solar cells using SnS HTL and TiO2 ETL, Sol. Energy 215 (2021) 64–76.
[37] M. Taguchi, et al., Obtaining a higher Voc in HIT cells, Prog. Photovoltaics Res. Appl. 13 (6) (2005) 481–488.
[38] M. Fox, Optical Properties of Solids, second ed., Oxford Master Series in Physics, 2010.
[39] M.M. Khatun, A. Sunny, S.R.A. Ahmed, Numerical investigation on performance improvement of WS2 thin-film solar cell with copper iodide as hole transport layer, Sol. Energy 224 (2021) 956–965.
[40] W. Shockley, W.T. Read, Statistics of the recombinations of holes and electrons, Phys. Rev. 87 (5) (1952) 835–842.
[41] A.E.H. Benzetta, M. Abderrezek, M.E. Djeghlal, Contribution to improve the performances of Cu2ZnSnS4 thin-film solar cell via a back surface field layer, Optik 181 (2019) 220–230.
[42] A.D. Adewoyin, M.A. Olopade, M. Chendo, Enhancement of the conversion efficiency of Cu2ZnSnS4 thin film solar cell through the optimization of some device parameters, Optik 133 (2017) 122–131.
[43] F.A. Jhuma, M.Z. Shaily, M.J. Rashid, Towards high-efficiency CZTS solar cell through buffer layer optimization, Materials for Renewable and Sustainable Energy 8 (1) (2019) 6.
[44] Y.P. Varshni, Temperature dependence of the energy gap in semiconductors, Physica 34 (1) (1967) 149–154.
[45] S.R.A. Ahmed, A. Sunny, S. Rahman, Performance enhancement of Sb2Se3 solar cell using a back surface field layer: a numerical simulation approach, Sol. Energy Mater. Sol. Cell. 221 (2021), 110919.